Corner flow in free liquid films

ROMAN STOCKER and A. E. HOSOI[1]

*Department of Applied Mathematics, Massachusetts Institute of Technology, 77 Massachusetts Avenue,
Cambridge, MA 02139, U.S.A.; e-mail: stocker@math.mit.edu;* [1]*Department of Mechanical Engineering,
Hatsopoulos Microfluids Laboratory, Massachusetts Institute of Technology, 77 Massachusetts Avenue,
Cambridge, MA 02139, U.S.A.; e-mail: peko@mit.edu*

Abstract. A lubrication-flow model for a free film in a corner is presented. The model, written in the hyperbolic
coordinate system $\xi = x^2 - y^2$, $\eta = 2xy$, applies to films that are thin in the η-direction. The lubrication
approximation yields two coupled evolution equations for the film thickness and the velocity field which, to lowest
order, describes plug flow in the hyperbolic coordinates. A free film in a corner evolving under surface tension
and gravity is investigated. The rate of thinning of a free film is compared to that of a film evolving over a solid
substrate. Viscous shear and normal stresses are both captured in the model and are computed for the entire flow
domain. It is shown that normal stress dominates over shear stress in the far field, while shear stress dominates
close to the corner.

Key words: corner, hyperbolic coordinates, lubrication theory, thin film

1. Introduction

Free liquid films are the basic structural element of foams, emulsions and many colloidal systems [1], with widespread applications in industrial and biological processes. Foams are used in important areas such as food and chemical industries, fire-fighting and structural material science [2]. The structure and stability of these systems intrinsically depends on the dynamics of the liquid films. Investigation of thin films typically relies on the use of reduced models, such as lubrication theory, which can be applied when the flow geometry is characterized by two widely disparate length scales. The full governing equations can then be reduced to one or two nonlinear evolution equations, which can be solved numerically or analyzed to predict the formation of singularities leading to rupture [3]. Advantages of these reduced models over an entirely numerical approach include avoiding the complexity of the original free-boundary problem, computational savings and a deeper understanding of the underlying physics. These advantages have sparked the development of a large literature on lubrication models, as reviewed by Oron, Davis and Bankoff [4].

A free film is bounded by two liquid-gas interfaces [4]. Because the symmetric mode (also known as the varicose or 'squeeze' mode) is most unstable [5], a symmetry condition is typically applied at the film's centerline [5, 6]. The evolution of a thinning liquid film involves roughly two stages. When the thickness of the film is relatively large, the dominant forces determining the evolution are surface tension and gravity, counteracted by viscous dissipation. At this stage, thinning typically occurs due to the drainage of liquid out of the film. Eventually, the film thickness diminishes to a scale (10–100 nm, [4]) at which long-range molecular van der Waals forces and electric double-layer repulsive forces become important. At this scale, in the absence of double-layer forces, surface tension yields to van der Waals forces
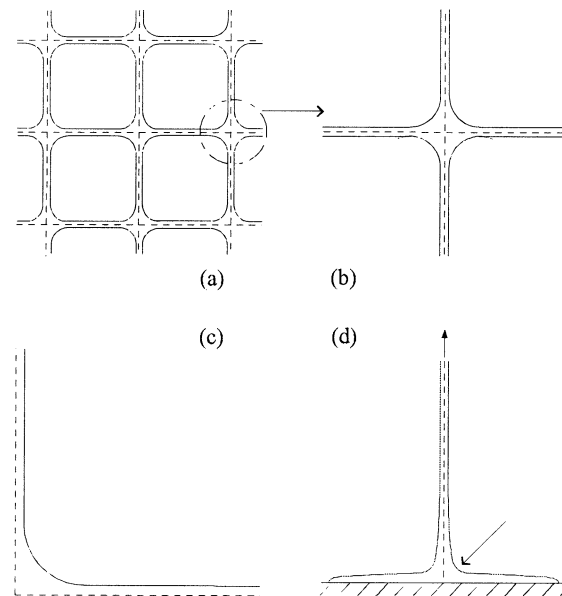
Figure 1. (a) An idealized model of a coarsening foam as a periodic array of bubbles (*e.g.* [11]). The solid lines represent the boundaries between the air bubbles and the liquid phase. (b) A close-up of the corner region formed by two intersecting liquid filaments. (c) The flow geometry under investigation. (d) Stretching of liquid threads. This application arises in rheological experiments, when a liquid thread is pulled in the direction of the vertical arrow. The arrow near the corner indicates the region where 'fishbone' instabilities are observed experimentally for viscoelastic fluids [27]. Dashed lines represent axes of symmetry in all panels.

[7], and random surface corrugations or defects grow causing film rupture [8]. This regime has been investigated in depth using both linear and nonlinear stability analyses [5–7, 9, 10]. Nonlinearities act to accelerate rupture, in both free films [5], and films on a solid substrate [7].

Previous studies have investigated unidirectional film flow. This simple unidirectional-flow approximation is often invoked in models of rupture of the liquid bridge between two gas bubbles in a foam [4]. While foam dynamics are influenced by several complicated factors, such as evaporation, contamination, and gradients in surface tension, rupture is observed in the simplest case of a constant surface tension and van der Waals forces [5, 7]. On the other hand, such a unidirectional model completely neglects the abrupt change in direction the film undergoes in an actual foam. A somewhat more realistic model in this respect idealizes the foam as a two-dimensional periodic array of air bubbles immersed in a liquid matrix, as done by Pozrikidis [11]. Such a foam is sketched in Figure 1a. When the bubbles expand due, for example, to a drop in ambient pressure, liquid drains into corner-like regions known as Plateau borders, eventually leading to the break-up of the thin films separating adjacent bubbles. A close-up of one of these corner regions is sketched in Figure 1b. While progress has been made towards understanding the evolution of these two-dimensional foams numerically using boundary-integral methods [11], no satisfying description has yet been given of the structure of the thin films separating the Plateau borders that accurately predicts rupture. In Pozrikidis' model, for example, the film thickness decreases in time in a power-law fashion, and rupture occurs only after an infinite time.

In this work, we suggest an alternative formulation to account for the corner-like geometry, based on the use of hyperbolic coordinates, which allows substantial analytical progress towards the determination of the flow in a Plateau border and attached liquid threads. We consider a region of flow forming an angle of $\pi/2$ and delimited on the left and bottom by symmetry planes as depicted in Figure 1c. We focus on the first stage of the development, involving the thinning and drainage of a free liquid film. While rupture is not addressed in this study, it is hoped that the present model will ultimately aid in predicting rupture times as well.

Lubrication theory fundamentally relies on a separation of length scales, with the film being considerably thinner in one of the coordinate directions. This amounts to requiring a small slope of the free surface. The primary obstacle associated with applying lubrication theory to the flow of a thin film in a corner is that, at least in Cartesian coordinates, the small slope requirement inevitably breaks down as the film negotiates the corner. In the literature, several methods have been attempted to bypass this limitation. None of them, however, tackles the issue directly. One approach argues that the effect of the sharp corner is small. This approach was taken successfully by Kalliadasis, Bielarz and Homsy [12] for the coating of microelectronic components, where the aim is to coat micron-sized trenches under the influence of surface tension. Kalliadasis and coworkers recognize that their lubrication model is expected to break down in the immediate vicinity of the sharp steps of the trench. Mazouchi and Homsy [13] investigated the same configuration assuming a two-dimensional free-surface Stokes flow (*i.e.*, without assuming a separation of length scales) using a boundary-integral method, and found good agreement with the lubrication theory. This indicates that the region around the sharp step where lubrication breaks down is small, and its effect on the levelling of the trench subdominant, validating the assumptions of the earlier authors. On the other hand, it is not clear that this is always the case for sharp topography, particularly for flows in which the dominant physics and instabilities occur exclusively in the corner.

A second method of bypassing the inability of existing lubrication models to describe flow around a sharp corner is to use two separate solutions and apply a matching criterion. This mimics the classic Landau-Levich problem [14] of an infinite plate pulled out from a deep bath. Landau and Levich derived separate expressions for the thin film coating the plate and the static meniscus in the deep pool, and closed the problem by matching the curvature. The same approach was adopted by Braun, Snow and Naire [15], for a symmetry, instead of a no-slip, boundary condition across the vertical axis. Braun and coworkers recognize the limitation of this approach and suggest it would be desirable to have a solution which ties together the two flow regions. While their flow configuration differs from ours in that we have two thin films, instead of a thin film and a deep bath, the issue of avoiding a matching criterion remains.

A third approach, developed for flow over topography, involves adopting a locally orthogonal coordinate system that naturally fits an arbitrarily curved substrate, as done by Schwartz and Weidner [16] and Roy, Roberts and Simpson [17]. The shape of the free surface is then dictated by the competition between the substrate, which impresses its shape onto the interface – effectively contributing an additional capillary pressure – and surface tension, which tends to flatten the free surface, ironing out short-wavelength irregularities and driving the solution to the stable minimum-energy configuration [12]. The long-term evolution is determined primarily by the topography of the substrate [17]. While these methods are very general, they are still unable to describe sharp features, as the evolution equations contain the gradient of the curvature of the substrate, which is singular at a sharp corner. Indeed, no attempt was made in [16] or [17] to model sharp features. In [18] (hereafter denoted as SH), we consider the

evolution of a thin film bounded by a solid corner and show that, by retaining the full position-dependent terms that arise in the hyperbolic coordinate system, we avoid this singularity which allows lubrication theory to be extended to flow around sharp topography.

Our choice of coordinate system overcomes these problems and provides a single solution over the whole flow domain, without the need for matching. The model is based on the idea that the liquid film in Figure 1c is thin everywhere, if its thickness is measured as the 'distance' from the free surface to the two axes of symmetry. This led us to adopt a hyperbolic coordinate system, which naturally fits the corner. We will thus extend the lubrication theory to this flow configuration using hyperbolic coordinates. In SH, we show – for a no-slip boundary condition – that in this new coordinate system lubrication theory leads to a single evolution equation for the film thickness, following the exact integration of the mass conservation equation. Here we extend this idea to the case of symmetry boundary conditions, appropriate for the varicose mode of free films. Instead of a single evolution equation, we obtain two coupled equations for the thickness of the film and its lowest-order velocity field, which describes plug flow in the hyperbolic coordinates. Two equations are also required for a free film in the unindirectional-flow case, as pointed out by Erneux and Davis [5], because the leading-order boundary conditions are not sufficient to uniquely prescribe the velocity profile: both the symmetry condition at the symmetry axis and the tangential-stress condition at the free surface require the transverse gradient of the velocity profile to vanish, leaving the magnitude of the plug flow velocity unspecified. The problem is closed by resorting to the next-order tangential-stress boundary condition, which yields a second evolution equation.

The applications of the no-slip case and the symmetry case are rather different, as outlined above, as is the dominant physics. Shear stress is expected to dominate over normal stress in the no-slip case (SH) and vice versa for unidirectional free films. In this paper we compute and compare viscous shear and normal stresses for the entire flow field of a free film. We can thus show that, as expected, normal viscous stresses dominate far away from the corner. On the other hand, close to the corner the sharp change in direction of the film causes shear stress to be larger than normal stress. This differs from the unidirectional-flow case treated in most lubrication models with a symmetry boundary condition (where shear is typically neglected), and is expected to be important in understanding the rupture of free films in corner geometries.

After establishing the governing equations in the hyperbolic coordinate system in the next section, lubrication theory is applied in Section 3 to derive the two evolution equations. The numerical scheme used to solve these equations is described in Section 4. Results are given in Section 5 and discussed in Section 6.

2. Hyperbolic coordinates

2.1. Governing equations in vector form

We consider free-surface flow in a corner bounded by two symmetry planes, as sketched in Figure 1c. The governing equations are

$$\frac{\nabla p}{\rho} = \nu \nabla^2 \boldsymbol{u} - g\hat{\mathbf{k}}, \qquad \nabla \cdot \boldsymbol{u} = 0, \tag{1}$$

where $\boldsymbol{u}$ is the velocity field, p the pressure, ν the kinematic viscosity, ρ the density, g the acceleration of gravity, and $\hat{\boldsymbol{k}}$ the unit vertical vector, pointing upwards. Since this work is concerned with low Reynolds number flow, inertia has been neglected in Equation (1). We
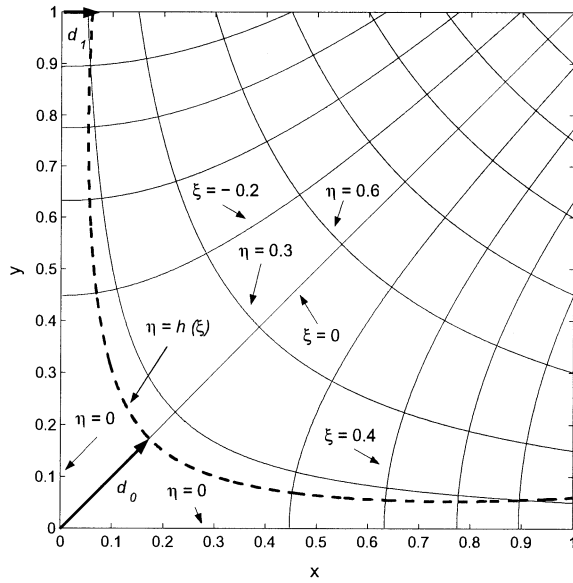
Figure 2. The coordinate system $\xi = x^2 - y^2$, $\eta = 2xy$. Also shown is a sketch of the free surface $\eta = h(\xi)$ of a thin film (dashed line). The thickness of the film at $\xi = -1$ and $\xi = 0$ is denoted as d_1 and d_0, respectively.
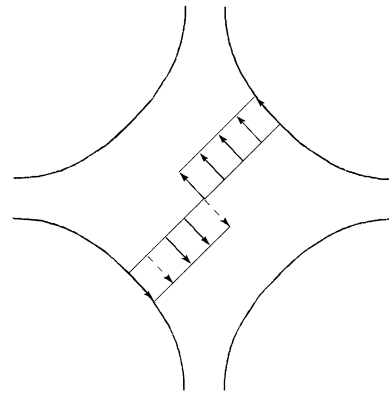
Figure 3. Sketch of the singularity in the lowest order velocity field (plug flow) of a free film in a corner. The dashed lines indicate axes of symmetry. The velocity field at $\xi = 0$ (*i.e. $x = y$*) has a discontinuity at the origin unless $U(\xi = 0) = 0$. As the successful integration of the film profile shows, this singularity is subdominant in the evolution of the film. The velocity profile is shown for only two of the four quadrants for the sake of clarity.

consider two-dimensional systems, assuming no variation in the third direction. The two stress boundary conditions at the free surface are

$$\hat{\boldsymbol{n}} \cdot \boldsymbol{\Pi} \cdot \hat{\boldsymbol{n}} = \sigma \kappa, \qquad \hat{\boldsymbol{t}} \cdot \boldsymbol{\Pi} \cdot \hat{\boldsymbol{n}} = 0, \tag{2}$$

where $\hat{\boldsymbol{n}}$ and $\hat{\boldsymbol{t}}$ are the unit outward normal and tangent vectors, respectively, σ is the surface tension, and κ, is the curvature of the free surface. For a Newtonian fluid, the stress tensor is

$$\boldsymbol{\Pi} = 2\mu \frac{\nabla \boldsymbol{u} + (\nabla \boldsymbol{u})^T}{2} - p\boldsymbol{I}, \tag{3}$$

where $\mu = \rho \nu$ is the dynamic viscosity, $\boldsymbol{I}$ the identity matrix, and ^{T} indicates a transpose matrix. We will further impose conservation of mass and symmetry across the two planes defining the corner (see Figure 1c).

2.2. COORDINATE TRANSFORMATION

The fundamental idea behind our method is to exploit the fact that the film is thin everywhere when measured from the axes of symmetry. Cartesian coordinates (x, y) are clearly ill-suited to the lubrication approximation, as the film is not everywhere thin in one of the two coordinate directions. On the other hand, if viewed in the hyperbolic coordinate system,

$$\xi = x^2 - y^2, \qquad \eta = 2xy, \tag{4}$$

as shown in Figure 2, the film can be treated as thin everywhere in the η direction. Note that the two orthogonal planes defining the corner now correspond to $\eta = 0$, and η increases with x and y in the first quadrant. The coordinate ξ increases along the corner from large y towards large x, in the shape of hyperbolas. The change of coordinates (4) is a special case of the analytical conformal mapping for a corner of angle π/n:

$$\xi = \mathfrak{Re}\left[(x + \mathrm{i}y)^n\right], \qquad \eta = \mathfrak{Im}\left[(x + \mathrm{i}y)^n\right], \tag{5}$$

where $\mathfrak{Re}$ and $\mathfrak{Im}$ indicate the real and imaginary part, respectively. The derivations become cumbersome for arbitrary n. Here, we pursue the case of a square corner ($n = 2$).

Since the mapping (Equation (4)) is conformal, the (ξ, η) coordinate system (4) is orthogonal and the scale factors h_1 and h_2 associated with the ξ and η directions are equal:

$$h_1 \equiv \left[\left(\frac{\partial x}{\partial \xi}\right)^2 + \left(\frac{\partial y}{\partial \xi}\right)^2\right]^{1/2} = \frac{1}{2\sqrt{r}} = \left[\left(\frac{\partial x}{\partial \eta}\right)^2 + \left(\frac{\partial y}{\partial \eta}\right)^2\right]^{1/2} \equiv h_2, \tag{6}$$

and will be denoted by $s = h_1 = h_2$. The derivatives of (x, y) with respect to (ξ, η) are given in the Appendix and $r \equiv (\xi^2 + \eta^2)^{1/2} = x^2 + y^2$. The coordinate transformation (4) is therefore singular at the origin. However, this does not present a problem since, if we exclude rupturing, the free surface never passes through the origin. The consequences of this singularity will be further explored after the evolution equations have been derived.

The gradient, divergence, and Laplacian in the hyperbolic coordinates are, respectively (*e.g.* [19, Chapter 2]):

$$\nabla p = \frac{1}{s}\frac{\partial p}{\partial \xi}\hat{\boldsymbol{\xi}} + \frac{1}{s}\frac{\partial p}{\partial \eta}\hat{\boldsymbol{\eta}}, \tag{7a}$$

$$\nabla \cdot \boldsymbol{u} = \frac{1}{s^2}\left[\frac{\partial(u\,s)}{\partial \xi} + \frac{\partial(v\,s)}{\partial \eta}\right], \tag{7b}$$

$$\nabla^2 \boldsymbol{u} = \nabla \cdot \nabla \boldsymbol{u} = \frac{1}{s^2}\left[\frac{\partial}{\partial \xi}\left(\frac{\partial \boldsymbol{u}}{\partial \xi}\right) + \frac{\partial}{\partial \eta}\left(\frac{\partial \boldsymbol{u}}{\partial \eta}\right)\right]. \tag{7c}$$

where $\hat{\boldsymbol{\xi}}$ and $\hat{\boldsymbol{\eta}}$ are the unit vectors in the hyperbolic coordinates and $\boldsymbol{u} = u\hat{\boldsymbol{\xi}} + v\hat{\boldsymbol{n}}$ is the velocity field.

2.3. GOVERNING EQUATIONS IN HYPERBOLIC COORDINATES

The governing Equations (1) in the coordinate system (ξ, η) read

$$\frac{\partial u}{\partial \xi} + \frac{\partial v}{\partial \eta} + f_1 u + f_2 v = 0, \tag{8a}$$

$$\frac{1}{\rho}\frac{\partial p}{\partial \xi} = \frac{\nu}{s}\left[\frac{\partial^2 u}{\partial \xi^2} + \frac{\partial^2 u}{\partial \eta^2} - \frac{1}{r^2}\left(\eta\frac{\partial v}{\partial \xi} - \xi\frac{\partial v}{\partial \eta} + \frac{u}{4}\right)\right] - g\frac{\partial y}{\partial \xi}, \tag{8b}$$

$$\frac{1}{\rho}\frac{\partial p}{\partial \eta} = \frac{\nu}{s}\left[\frac{\partial^2 v}{\partial \xi^2} + \frac{\partial^2 v}{\partial \eta^2} - \frac{1}{r^2}\left(-\eta\frac{\partial u}{\partial \xi} + \xi\frac{\partial u}{\partial \eta} + \frac{v}{4}\right)\right] - g\frac{\partial y}{\partial \eta}. \tag{8c}$$

The first two terms in the square brackets are the Laplacian of the scalar quantities u and v, while the remaining terms arise because the unit vectors $\hat{\boldsymbol{\xi}}$ and $\hat{\boldsymbol{\eta}}$ are position-dependent (see SH). The functions f_1, f_2, $\partial y/\partial \xi$ and $\partial y/\partial \eta$ depend only on the position (ξ, η), as defined in the Appendix. The consequences of this explicit position-dependence of the governing equations on the development of a lubrication theory will be discussed later in Section 6.

It is worth noting that an exact solution for viscous stagnation-point flow is given by Moffatt [20], who describes the flow field near sharp corners of any angle with various boundary conditions using the stream function ψ in polar coordinates $(\hat{r}, \theta)$. For a free fluid in a square corner, Moffatt's (antisymmetric) stream function is $\psi = \hat{r}^2 \cos(2\theta) = x^2 - y^2 = \xi$, indicating that hyperbolic coordinates are indeed the natural choice to describe these flows. The symmetric solution is $\psi = \eta$. As expected, both the symmetric and antisymmetric solutions satisfy Equation (8). What distinguishes our solution from Moffatt's is the presence of a free surface.

Using the expression for a Newtonian stress tensor given in Equation (A5) together with (A4), we write the stress boundary condition (2) as

$$
-p + \frac{2\mu}{s(1 + h'^2)} \left[\frac{\partial v}{\partial \eta} - \frac{\xi u}{2r^2} + h'^2 \left(\frac{\partial v}{\partial \xi} - \frac{\eta v}{2r^2} \right) \right.
$$
$$
\left. -h' \left(\frac{\partial v}{\partial \xi} + \frac{\partial u}{\partial \eta} + \frac{\eta u + \xi v}{2r^2} \right) \right] = \sigma \kappa, \tag{9a}
$$

$$
2h' \left(\frac{\partial v}{\partial \eta} - \frac{\partial u}{\partial \xi} + \frac{\eta v - \xi u}{2r^2} \right) + (1 - h'^2) \left(\frac{\partial v}{\partial \xi} + \frac{\partial u}{\partial \eta} + \frac{\eta u + \xi v}{2r^2} \right) = 0, \tag{9b}
$$

evaluated at the free surface $\eta = h$. A prime denotes differentiation with respect to ξ. The curvature, κ, is given by

$$
\kappa = -\nabla \cdot \hat{\boldsymbol{n}} = \frac{h''}{s(1 + h'^2)^{3/2}} + \frac{h' f_1 - f_2}{s(1 + h'^2)^{1/2}}. \tag{10}
$$

The symmetry boundary condition requires

$$
\frac{\partial u}{\partial \eta} = v = 0 \qquad (\eta = 0). \tag{11}
$$

The last condition imposed is conservation of mass (or, equivalently, volume, since we assume a constant density)

$$
\frac{\partial A}{\partial t} + \frac{\partial Q}{\partial \xi} = 0, \tag{12}
$$

where

$$
A = \int_0^{h(\xi)} s^2 \mathrm{d}\eta, \qquad Q = \int_0^{h(\xi)} u(\xi, \eta) s \mathrm{d}\eta. \tag{13}
$$

We will show that Equations (13) can be integrated analytically for a free film, allowing mass conservation to be satisfied exactly. In the next section, lubrication theory is applied to the full governing equations (8), (9) and (12) to obtain two coupled evolution equations for the film thickness and the lowest order velocity field.

3. Lubrication theory

3.1. THE REDUCED EQUATIONS

In this section, we derive the evolution equations for a thin layer of liquid evolving under surface tension and gravity in a corner region delimited by two axes of symmetry. We first rescale the governing equations (8), (9) and (12) by writing

$$\xi = L\tilde{\xi}, \qquad u = \mathcal{U}\tilde{u}, \qquad t = T\tilde{t} = \sqrt{L}\tilde{t}/\mathcal{U}, \tag{14a}$$

$$\eta = H\tilde{\eta}, \qquad v = \mathcal{V}\tilde{v}, \qquad p = P\tilde{p}, \tag{14b}$$

where a tilde denotes dimensionless variables. Since ξ and η are quadratic in the original coordinates (x, y), L and H have dimensions of length squared, and represent the characteristic 'length' and 'thickness' of the film in the hyperbolic coordinate system. $\mathcal{U}$ and $\mathcal{V}$ are characteristic velocities along and across the layer, respectively, and P is the pressure scale. In order to include the case of zero gravity, a characteristic velocity along ξ is defined in terms of viscosity and surface tension, as $\mathcal{U} = \tilde{\sigma}/\mu$, where $\tilde{\sigma} = \varepsilon\sigma$. The latter rescaling of surface tension ensures that capillary forces are retained in the equations to leading order. Thus, the characteristic time $T = \sqrt{L}/\mathcal{U}$ required for a fluid parcel with velocity $\mathcal{U}$ to travel the physical length $\sqrt{L}$ of the layer, is $T = \mu\sqrt{L}/\tilde{\sigma}$. Since only dimensionless variables will be used from now on, unless otherwise stated, the tildes are dropped.

In the lubrication limit, we assume that the parameter $\varepsilon = H/L$ is small, and expand the dependent variables u, v and p in powers of ε, as

$$u = u_0 + \varepsilon^2 u_2 + O(\varepsilon^4), \tag{15a}$$

$$v = v_0 + \varepsilon^2 v_2 + O(\varepsilon^4), \tag{15b}$$

$$p = p_0 + \varepsilon^2 p_2 + O(\varepsilon^4). \tag{15c}$$

Note that this is equivalent to expanding in powers of $\text{Ca}^{1/3} \ll 1$ where $\text{Ca} = \mu\mathcal{U}/\sigma$ is the Capillary number. Quantities dependent on the position (ξ, η) are also made dimensionless (f_1 scales like L, f_2 like ε/L, and s like $1/\sqrt{L}$). The position-dependent terms f_1, f_2, and s could also in principle be expanded in powers of ε. However, this leads to a singularity at $\xi = 0$. We therefore choose to retain in full all terms that depend on position alone. We will later discuss the rationale and consequences of this approach.

The continuity equation (8a) yields a relation between the two velocity scales, $\mathcal{V} = \varepsilon\mathcal{U}$. The momentum equation (8b) along ξ suggests a pressure scale $P = \tilde{\sigma}/\sqrt{L}$. The Bond number $\text{Bo} = \rho g L/\tilde{\sigma}$ expresses the relative importance of gravity and surface tension. Equating terms of like order in ε, we obtain the following system at $O(1)$:

$$\frac{\partial u_0}{\partial \xi} + \frac{\partial v_0}{\partial \eta} - \frac{\xi}{2r^2}u_0 = 0, \tag{16a}$$

$$\frac{\partial^2 u_0}{\partial \eta^2} = 0, \tag{16b}$$

$$\frac{\partial p_0}{\partial \eta} = 2\sqrt{r}\frac{\partial^2 v_0}{\partial \eta^2} - \frac{2\xi}{r^{3/2}}\frac{\partial u_0}{\partial \eta} - \text{Bo}\frac{\partial y}{\partial \eta}, \tag{16c}$$

$$-p_0 + 4\sqrt{r}\left(\frac{\partial v_0}{\partial \eta} - \frac{\xi u_0}{2r^2} - h'\frac{\partial u_0}{\partial \eta}\right) = \kappa \quad (\eta = h), \tag{16d}$$

$$\frac{\partial u_0}{\partial \eta} = 0 \qquad (\eta = h), \tag{16e}$$

$$\frac{\partial u_0}{\partial \eta} = v_0 = 0 \qquad (\eta = 0), \tag{16f}$$

representing continuity, conservation of momentum along ξ and η, normal and tangential stress conditions, and the symmetry boundary condition, respectively. Here, we have used the rescaled expression for r:

$$r = \left(\xi^2 + \varepsilon^2\eta^2\right)^{1/2}. \tag{17}$$

At $O(\varepsilon^2)$, we obtain

$$\frac{\partial p_0}{\partial \xi} = 2\sqrt{r}\left[\frac{\partial^2 u_0}{\partial \xi^2} + \frac{\partial^2 u_2}{\partial \eta^2} + \frac{1}{r^2}\left(\xi\frac{\partial v_0}{\partial \eta} - \frac{u_0}{4}\right)\right] - \mathrm{Bo}\frac{\partial y}{\partial \xi}, \tag{18a}$$

$$2h'\left(\frac{\partial v_0}{\partial \eta} - \frac{\xi u_0}{2r^2} - \frac{\partial u_0}{\partial \xi}\right) + \frac{\partial v_0}{\partial \xi} + \frac{\eta u_0 + \xi v_0}{2r^2} + \frac{\partial u_2}{\partial \eta} - h'^2\frac{\partial u_0}{\partial \eta} = 0 \quad (\eta = h), \tag{18b}$$

$$\frac{\partial u_2}{\partial \eta} = v_2 = 0 \qquad (\eta = 0), \tag{18c}$$

representing conservation of momentum along ξ, the tangential stress condition and the symmetry boundary condition, respectively.

We chose to retain the full expression for curvature (Equation (10)), as Eggers and Dupont [21] showed that this ensures that the potential energy associated with the lubrication solution is the same as that of the full equations, so that the static equilibrium solutions of the model are in fact exact. While this is often customary procedure, it is not a strictly necessary one in this case, as the film profile computed using the approximated curvature converges to that obtained with the full curvature.

3.2. Evolution equations

The reduced momentum equation (16b) along ξ, together with the boundary conditions (16e,f), yields $u_0 = U(\xi)$. Thus, the leading-order velocity field is one of plug flow in the hyperbolic coordinates. We now substitute $u_0 = U(\xi)$ in the mass conservation equation (12), using the integrals

$$\frac{\partial}{\partial t}\int_0^h s^2 \mathrm{d}\eta = \frac{\partial}{\partial t}\int_0^h \frac{\mathrm{d}\eta}{4(\xi^2 + \varepsilon^2\eta^2)^{1/2}} = \frac{1}{4(\xi^2 + \varepsilon^2 h^2)^{1/2}}\frac{\partial h}{\partial t}, \tag{19a}$$

$$\int_0^h u_0 s \mathrm{d}\eta = \frac{Uh}{2|\xi|^{1/2}}{}_2F_1\left(\frac{1}{2}, \frac{1}{4}; \frac{3}{2}; -\frac{\varepsilon^2 h^2}{\xi^2}\right), \tag{19b}$$

${}_2F_1$ is a hypergeometric function [22, Chapter 15]. This yields the first evolution equation

$$\frac{1}{4(\xi^2 + \varepsilon^2 h^2)^{1/2}}\frac{\partial h}{\partial t} + \frac{\partial}{\partial \xi}\left[\frac{Uh}{2|\xi|^{1/2}}{}_2F_1\left(\frac{1}{2}, \frac{1}{4}; \frac{3}{2}; -\frac{\varepsilon^2 h^2}{\xi^2}\right)\right] = 0, \tag{20}$$

linking the film thickness $h(\xi, t)$ to the lowest order velocity field $U(\xi, t)$. To solve for h and U a second equation is required. Before solving the $O(\varepsilon^2)$ system, we compute v_0 and p_o. We find v_0 from the continuity equation (16a):

$$v_0 = -U'\eta + \frac{U}{2\varepsilon}\arctan\left(\frac{\varepsilon\eta}{\xi}\right). \tag{21}$$

The pressure p_0 is obtained by integrating Equation (16c) from η to h and making use of (16d), resulting in

$$p_0 = g_1 + \frac{4U\xi}{3r^{3/2}} - \kappa + \text{Bo}\left[y|_h - y|_\eta\right], \tag{22}$$

where y is given in terms of ξ and η in the Appendix, the vertical bar indicates the value of η where a quantity is evaluated, and

$$g_1(\xi) = -4U'\left(\xi^2 + \varepsilon^2 h^2\right)^{1/4} - \frac{4U\xi}{3(\xi^2 + \varepsilon^2 h^2)^{3/4}} \tag{23}$$

is independent of η.

At $O(\varepsilon^2)$, we substitute Equations (21) and (22) in (18a) and rearrange, to obtain

$$\frac{\partial^2 u_2}{\partial \eta^2} = \frac{g_2(\xi) + g_1'(\xi)}{2\sqrt{r}} - U'' + \frac{11U + 20\xi U'}{12r^2} - \frac{3U\xi^2}{2r^4}, \tag{24}$$

where

$$g_2(\xi) = -\kappa' + \text{Bo}\frac{\partial y}{\partial \xi}\bigg|_h. \tag{25}$$

The curvature gradient κ' is

$$\kappa' = \frac{2\alpha}{\beta^3}h''' - \frac{6\varepsilon^2\alpha}{\beta^5}h'(h'')^2 - \frac{3(h - \xi h')(\xi + \varepsilon^2 hh')}{2\alpha^7\beta}, \tag{26}$$

where $\alpha = (\xi^2 + \varepsilon^2 h^2)^{1/4}$, $\beta = (1 + \varepsilon^2 h'^2)^{1/2}$, and

$$\frac{\partial y}{\partial \xi}\bigg|_h = \frac{1}{2\sqrt{2}\left(\sqrt{\xi^2 + \varepsilon^2 h^2} - \xi\right)^{1/2}}\left[\frac{\xi + \varepsilon^2 hh'}{\sqrt{\xi^2 + \varepsilon^2 h^2}} - 1\right]. \tag{27}$$

Equation (24) is integrated once making use of the boundary condition (18c) and of the indefinite integrals

$$\int \frac{1}{(\xi^2 + \varepsilon^2\eta^2)^{1/4}}d\eta = \frac{\eta}{|\xi|^{1/2}}{}_2F_1\left(\frac{1}{4}, \frac{1}{2}; \frac{3}{2}; -\frac{\varepsilon^2\eta^2}{\xi^2}\right), \tag{28a}$$

$$\int \frac{1}{\xi^2 + \varepsilon^2\eta^2}d\eta = \frac{1}{\varepsilon\xi}\arctan\left(\frac{\varepsilon\eta}{\xi}\right), \tag{28b}$$

$$\int \frac{1}{(\xi^2 + \varepsilon^2\eta^2)^2}d\eta = \frac{\eta}{2\xi^2 r^2} + \frac{1}{2\varepsilon\xi^3}\arctan\left(\frac{\varepsilon\eta}{\xi}\right). \tag{28c}$$

This yields an expression for $\partial u_2/\partial \eta$. The latter is evaluated at $\eta = h$ and substituted in Equation (18b), yielding the second evolution equation

$$-2U''h - 4U'h' - \frac{3hU}{4(\xi^2 + \varepsilon^2 h^2)} + \frac{h(g_2 + g_1')}{2|\xi|^{1/2}} {}_2F_1\left(\frac{1}{4}, \frac{1}{2}; \frac{3}{2}; -\frac{\varepsilon^2 h^2}{\xi^2}\right) +$$

$$+ \frac{1}{6\varepsilon}\left[\frac{U}{\xi} + 13U' + \frac{3U\xi}{2(\xi^2 + \varepsilon^2 h^2)}\right] \arctan\left(\frac{\varepsilon h}{\xi}\right) - \frac{U'\xi h}{2(\xi^2 + \varepsilon^2 h^2)} = 0. \tag{29}$$

We have thus obtained two coupled nonlinear partial differential equations – (20) and (29) – that describe the evolution of $h(\xi, t)$ and $U(\xi, t)$. Contrary to the no-slip case (SH), all integrals can be evaluated analytically in deriving the two evolution equations, simplifying the numerical integration. The expansion parameter ε can be related to the filling fraction F_R - representing the liquid fraction of the unit Cartesian box - both being a measure of the film thickness. Therefore, the dependence of the evolution equations on ε amounts to a dependence on the filling fraction F_R. Note that we could introduce a rescaled thickness $\hat{h} = \varepsilon h$ to confine the ε-dependence to the initial condition.

4. Numerical solution of the evolution equations

The numerical method used to integrate the evolution equations closely follows the one applied in the no-slip case (SH). Here, we briefly summarize the main points, and outline some differences. To avoid computing higher-order finite differences, we define an auxiliary variable $f = h''$. Denoting the flux (the term in square brackets in Equation (20)) as q, the numerical scheme becomes

$$F_i^{n+1} = \frac{1}{4[\xi_i^2 + \varepsilon^2 (h_i^{n+1})^2]^{1/2}} \frac{h_i^{n+1} - h_i^n}{\Delta t} + \frac{q_{i+1/2}^{n+1} - q_{i-1/2}^{n+1}}{(\Delta_i^+ - \Delta_i^-)/2} = 0, \tag{30a}$$

$$G_i^{n+1} = f_i^{n+1} - m_i^+ h_{i+1}^{n+1} - m_i h_i^{n+1} - m_i^- h_{i-1}^{n+1} = 0, \tag{30b}$$

and similarly for H_i^{n+1}, whose numerical expression is omitted for brevity. The subscript i denotes the i-th grid point of the non-uniform grid. The free surface is located at (ξ_i, h_i^{n+1}) at time step $n + 1$. Note that, due to the U/ξ singularity in Equation (29), as discussed in the following section, one must avoid choosing $\xi = 0$ as a grid point. The distance between grid point i and its two neighbors $i \pm 1$ is $\Delta_i^\pm = |\xi_{i\pm1} - \xi_i|$. First derivatives were approximated by centered differences, except at the boundaries, where a forward or backward difference was used. Second derivatives were computed on a three point stencil as a weighted average of the first forward and backward derivatives, as in Equation (30b), with $m_i^+ = 2/[\Delta_{i+1}(\Delta_{i+1} + \Delta_{i-1})]$, $m_i = -2/(\Delta_{i+1}\Delta_{i-1})$ and $m_i^- = 2/[\Delta_{i-1}(\Delta_{i+1} + \Delta_{i-1})]$. Equation (30a) was discretized in flux-conservative form in order to ensure numerical mass conservation. At each grid point only the outward flux $q_{i+1/2}$ was computed, while for the inward flux $q_{i-1/2}$, the outward flux of its left neighbor $(i - 1)$ was reused.

We use an adaptive time step based on a step-doubling algorithm [23, Section 16.2] to minimize the computational time. At each step, two solutions are computed, the first (S_B) by using the full time step Δt, the second (S_S) by taking two steps of length $\Delta t/2$. If the error $|S_B - S_S|$, averaged over all grid points, is larger than a specified tolerance (typically 10^{-4}), the step is rejected and repeated after halving the time step. Otherwise, the step is accepted
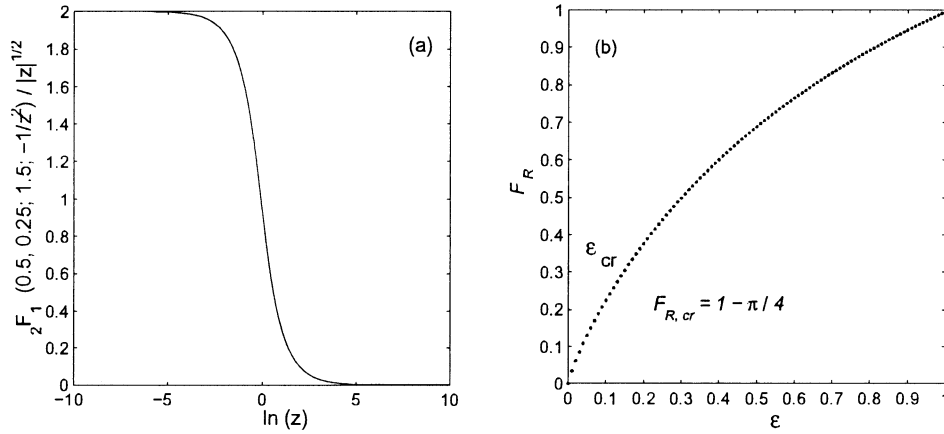
Figure 4. (a) The term containing the hypergeometric function appearing in both evolution equations, (20) and (29), with $z = |\xi|/(\varepsilon h)$. Its limit for $z \to 0$ is finite, proving that this term does not represent a singularity. (b) The filling fraction F_R as a function of the expansion parameter ε for the initial condition $h(\xi) = 1 + \xi^2$ used throughout this paper. The critical filling fraction and the corresponding critical value of ε are marked by the dashed lines.

and an extrapolated value $S = 2S_B - S_S$ of the solution is computed which achieves $O(\Delta t^2)$ accuracy. The next time step is then increased by a factor that is inversely proportional to the error. The solution at any step was found by solving Equations (30) implicitly with a Newton iteration procedure. The Jacobian of the functions F, G and H was computed analytically, resulting in an 11-diagonal matrix (five non-zero diagonals on each side of the main diagonal) that was inverted using the standard Gaussian elimination method for banded matrices [23, Section 2.4].

Four boundary conditions are required for the fourth-order system of differential equations consisting of Equations (20) and (29). Zero-flux and zero-slope conditions – amounting to a symmetry boundary condition in ξ – were imposed at both ends ($\xi = \pm 1$). These conditions must be expressed in the hyperbolic system. The boundary condition on the velocity U is derived from the definition of the flux, such that

$$U_i^{n+1} = q_i^{n+1} \left\{ \frac{h_i^{n+1}}{2|\xi_i|^{1/2}} {}_2F_1 \left[\frac{1}{2}, \frac{1}{4}; \frac{3}{2}; -\left(\frac{\varepsilon h_i^{n+1}}{\xi_i} \right)^2 \right] \right\}^{-1}, \tag{31}$$

to be applied at the first ($i = 1$) and last ($i = N$) grid points. The numerical scheme was implemented in Fortran, but the hypergeometric functions were more accurately evaluated using Matlab. More details on this aspect, as well as the grid and convergence tests, are given in SH.

5. Results

Before presenting numerical results, we discuss the singularity U/ξ in Equation (29). At $O(\varepsilon^2)$, U/ξ represents a physical singularity, which follows from the imposed symmetry condition and the plug flow velocity field, as sketched in Figure 3. Unless $U(\xi = 0) = 0$, a velocity discontinuity exists at the origin. To eliminate this singularity in the velocity derivative, one could extend the analysis to higher order. Instead, we proceed with the numerical
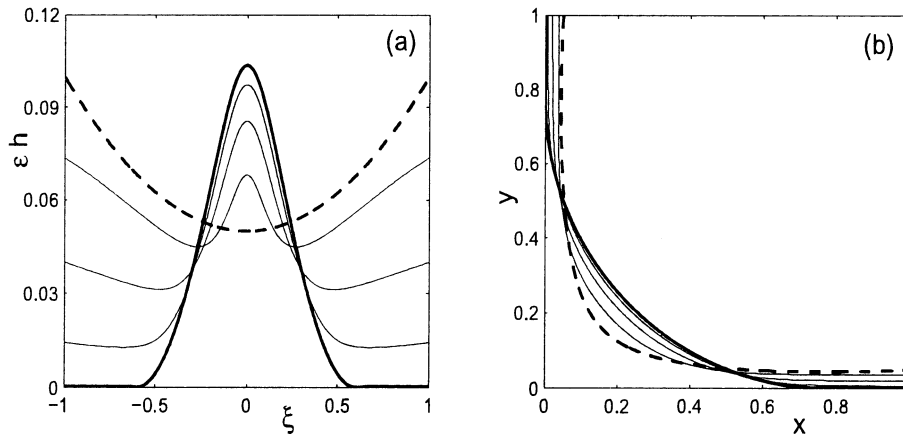
Figure 5. Evolution of a free film in the (ξ, η) plane (a) and in the (x, y) plane (b). The initial condition is $h = 1 + \xi^2$ and $\varepsilon = 0.05$. The dashed line represents the initial condition ($t = 0$), the thick solid line the steady state ($t = 100$). The intermediate profiles are at $t = 1.24$, 4.75 and 11.33.

integration (by simply ensuring that $\xi = 0$ is not a grid point), assuming that the integral contribution of the point-wise singularity to the overall evolution of the film is subdominant (mathematically, a portion of the integrand diverges, but its contribution to the integral is nevertheless small). U/ξ is the only singularity in the evolution equations, as the term $_2F_1/|\xi|^{1/2}$ (in Equations (20) and (29)), plotted in Figure 4a, has a finite limit as $|\xi| \to 0$. In traditional lubrication models written in the reference frame of the substrate [16, 17], a second singularity arises as the gradient of the *substrate* curvature enters the evolution equations. On the other hand, in our method only the gradient of the *interface* curvature (which is not singular) enters the equations, due to the particular choice of coordinates.

For all simulations we choose the initial condition $h(\xi) = 1 + \xi^2$, in the (ξ, η) plane. The relation between the filling fraction F_R and ε (Figure 4b) is obtained by integrating the initial condition. There is a critical value of the filling fraction $F_{R,cr} = 1 - \pi/4 \approx 0.215$ ($\varepsilon_{cr} \approx 0.094$), corresponding to the amount of liquid exactly fitting the unit square as a quarter of a circle.

Figure 5 shows the evolution of a free film under surface tension in a corner in both the (ξ, η) and the (x, y) planes. Both planes clearly illustrate the thinning of the threads as fluid is drawn towards the corner by surface tension. The steady state is a quarter of a circle adjacent to the corner, corresponding to the minimum potential energy configuration (*i.e.*, $g_2 = $ constant, see Equation (25)). The steady state is independent of the boundary condition at $\eta = 0$ and is therefore identical to the one verified experimentally in SH for a no-slip boundary condition. The rate of thinning, on the other hand, depends on the boundary condition at $\eta = 0$. In Figure 6, we present the time evolution of the film thickness at $\xi = -1$ (d_1), normalized by its initial value, for different values of ε. When $\varepsilon > \varepsilon_{cr} \approx 0.094$, the film evolves towards a quarter-of-a-circle steady state and d_1 approaches a finite value. For $\varepsilon < \varepsilon_{cr}$ the film thins at $\xi = -1$ until it reaches a scale at which new physics (*e.g.* van der Waals forces) must be included to continue the evolution.

It is interesting to compare the rate of thinning for a symmetry and a no-slip boundary condition. The two cases are compared in Figure 7. Figure 7a shows the evolution of the film thickness at $\xi = 0$ (d_0) for $\varepsilon = 0.05$. As expected, the evolution in the no-slip case is slower due to the drag exerted by the solid walls. The full circles in Figure 7a represent the time
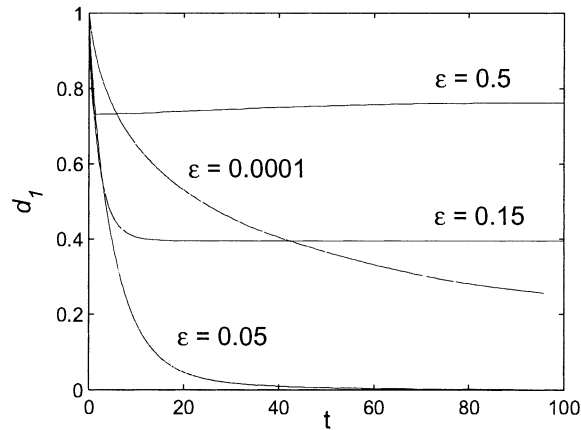
Figure 6. The film thickness d_1 at $\xi = -1$ (see Figure 2) as a function of time, normalized by its value at $t = 0$, for four values of ε. The initial condition is $h = 1 + \xi^2$. For $\varepsilon < \varepsilon_{cr} \approx 0.94$ a thinner film evolves comparatively slower. For $\varepsilon > \varepsilon_{cr}$ the film thickness does not tend to zero, as the filling fraction is larger than the critical value (see Figure 4b).
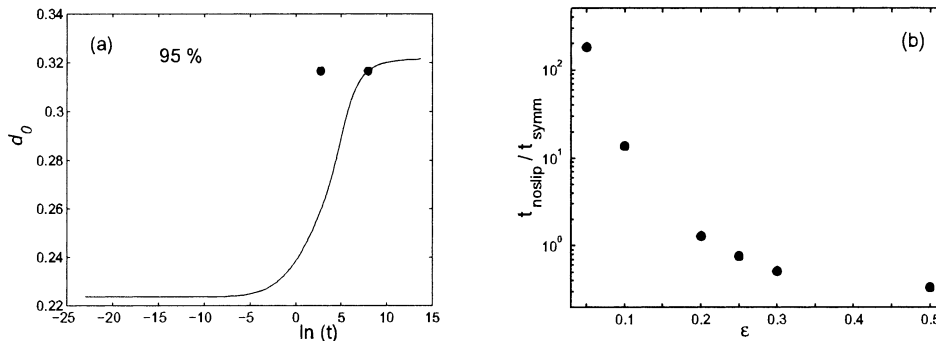

Figure 7. (a) The film thickness d_0 at $\xi = 0$ (see Figure 2) with $\varepsilon = 0.05$ as a function of time for a symmetry (dashed line) and a no-slip (solid line) boundary condition. The solution for the no-slip case is given in SH. The evolution is slower for a no-slip boundary condition. The circles mark the time at which the interface has travelled 95% of the distance to steady state. The ratio of this time for the no-slip and the symmetry boundary conditions is shown in panel (b) for several values of ε. As the film becomes thicker, the no-slip case becomes comparatively faster, since the retarding influence of the viscous drag exerted by the solid boundary diminishes.

taken by each film to reach 95% of its steady-state thickness at $\xi = 0$. The ratio of these times, $t_{\text{noslip}}/t_{\text{symm}}$, is plotted in Figure 7b for several values of ε. The thinner the film, the more pronounced the delay induced by the no-slip condition. The no-slip evolution is more than 100 times slower than the symmetry evolution for films thinner than $\varepsilon \approx 0.07$. For thicker films, the effect of a solid boundary is relatively less important.

When Bo $\neq 0$, the evolution is governed by a competition between surface tension and gravity. In SH, the effect of gravity was investigated both theoretically and experimentally for a no-slip condition, showing that, as the Bond number increases, more fluid drains down the vertical axis, forming a pool along the bottom. For both a free film and a film in a solid corner, the steady state corresponds to the solution of the Young-Laplace equation for a static meniscus [24, Paragraph 60]. The latter coincides with our evolution equations in the limit $U = \partial h/\partial t = 0$. On the other hand, the rate of thinning depends on the boundary condition at $\eta = 0$, as already shown in Figure 7. For a free film, Figure 8 shows the time, $t_{0.05}$, for the
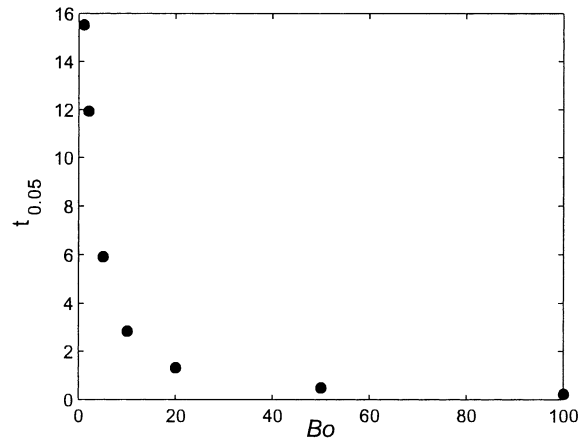
Figure 8. The influence of gravity on the evolution of a free film in a corner for $\varepsilon = 0{\cdot}01$. $t_{0.05}$ represents the time taken by the thickness of the film d_1 at $\xi = -1$ (see Figure 2) to reach 5% of its initial value. For Bo $= 0$, $t_{0.05} = 56{\cdot}3$. As Bo is increased, the film thins faster and forms a larger horizontal pool at the bottom (see also SH).

thickness at $\xi = -1$ (d_1) to reach 5% of its initial value for several Bond numbers. As the Bond number increases, the rate of thinning along the vertical axis increases, with a ten-fold decrease in $t_{0.05}$ for Bo $= 10$ over the case Bo $= 0$. It is important to note that, in the current configuration, 'gravity' should be interpreted as a generalized body force that satisfies all of the symmetry conditions. While the vertical axis presents no complications, the symmetry condition across the horizontal axis implies that this body force acts 'downward' for $y > 0$ and 'upward' for $y < 0$. This issue vanishes for physical scenarios involving mixed boundary conditions such as the vertical stretching of a viscoelastic fluid (as illustrated in Figure 1d, to be discussed in Section 6). In this stretching geometry, a symmetry condition is required for $\xi < 0$ ($y > x$) and a no-slip condition is required for $\xi > 0$ ($x > y$). Thus there is no contradiction between the symmetry condition across the y-axis and the effects of gravity as the two are aligned.

We can use the numerical solution $U(\xi, t)$ to quantify the relative importance of shear and normal stresses. Traditional lubrication models for free films [21] are based on the *assumption* that normal stress dominates over shear stress. The resulting plug flow velocity field clearly has no shear. The opposite is true for films over solid substrates, where shear is introduced by the solid boundary. These assumptions are in general correct for unidirectional films. In a corner region, the balance between shear and normal stresses is set by the competition between the boundary condition – symmetry or no-slip – and the geometry of the flow. The latter inevitably introduces some shear by forcing the film to undertake a sharp change in direction. If the corner walls are physical boundaries (no-slip case), these two effects reinforce each other, and shear stress is expected to dominate over normal stress everywhere. For a free film, on the other hand, the shear stress due to the geometry could potentially be comparable to the normal stress favoured by the symmetry boundary condition. In particular, we expect shear stress to be important close to the corner. While the lowest order velocity is one of plug flow, it should be noted that this is plug flow in the hyperbolic coordinates, which does not by itself imply that the flow is predominantly extensional.

To investigate this issue, we compute the viscous normal stress E and the viscous shear stress S (for unit viscosity). Using Cartesian velocities (u_x and u_y), E (S) is defined as half the
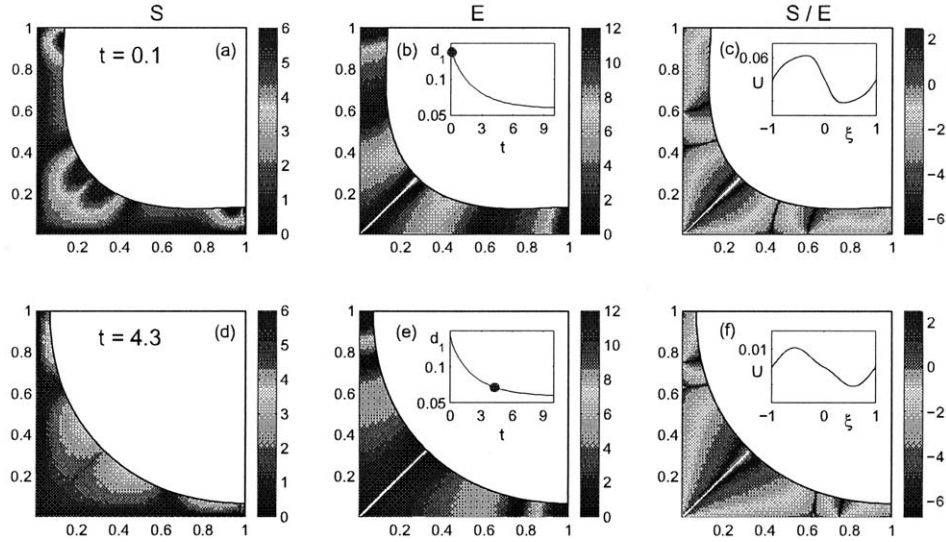
Figure 9. Contours of the shear stress S (a and d), the normal stress E (b and e), and their ratio S/E (c and f) for a free film in a corner with $\varepsilon = 0\cdot15$. An early ($t = 0\cdot1$: a,b,c) and a late stage ($t = 4\cdot3$: d,e,f) of the evolution are shown. The instantaneous velocity profile $U(\xi)$ is shown in the insets of (c) and (f). S and E have been normalized by the instantaneous maximum velocity U_{max}. The thickness of the film d_1 at $\xi = -1$ (see Figure 2) is shown in the insets of (b) and (e). Its instantaneous value, represented by the full circles, is an indicator of how far the film has evolved towards steady state.

sum of the absolute values of the diagonal (off-diagonal) elements of the rate of strain tensor $(\nabla \boldsymbol{u} + (\nabla \boldsymbol{u})^T)/2$. Thus, $S = |\partial u_x/\partial y + \partial u_y/\partial x|/2$ and $E = (|\partial u_x/\partial x| + |\partial u_y/\partial y|)/2 = |\partial u_x/\partial x|$, where we have used the continuity equation, $\partial u_y/\partial y = -\partial u_x/\partial x$, in calculating E. Absolute values are considered since we are interested in the magnitude of the stress. S and E can be computed from the stress tensor $\boldsymbol{\Pi}$ in hyperbolic coordinates (Equation (A5)) as

$$S = |\hat{\boldsymbol{j}} \cdot \boldsymbol{\Pi} \cdot \hat{\boldsymbol{k}}|, \qquad E = |\hat{\boldsymbol{j}} \cdot \boldsymbol{\Pi} \cdot \hat{\boldsymbol{j}}|, \tag{32}$$

where the unit Cartesian vectors $\hat{\boldsymbol{j}}$ and $\hat{\boldsymbol{k}}$ are given in Equation (A7). Using the lowest order velocity field $u = u_0 = U(\xi)$ and $v = v_0$ from Equation (21), we find

$$S(\xi, \eta) = \frac{2}{r^{1/2}} \left| -U'' \xi \eta \varepsilon - U' \left(2\varepsilon \eta - \frac{\xi}{2} \arctan \frac{\varepsilon \eta}{\xi} + \frac{\xi^2 \varepsilon \eta}{2r^2} \right) + \frac{\xi^2 U}{4\varepsilon r^2} \arctan \frac{\varepsilon \eta}{\xi} \right|, \tag{33a}$$

$$E(\xi, \eta) = \frac{2}{r^{1/2}} \left| -U'' \varepsilon^2 \eta^2 + U' \left(2\xi + \frac{\varepsilon \eta}{2} \arctan \frac{\varepsilon \eta}{\xi} - \frac{\xi^2 \varepsilon^2 \eta^2}{2r^2} \right) + \frac{\xi \eta \varepsilon U}{4r^2} \arctan \frac{\varepsilon \eta}{\xi} \right|. \tag{33b}$$

Figure 9 shows contours of S, E and S/E at two instants for $\varepsilon = 0\cdot15$. As both S and E are proportional to the plug flow velocity U (shown in the inset of Figure 9c,f), they were normalized by the instantaneous maximum velocity, U_{max}, to facilitate comparison along different times. The insets in Figure 9b,e provide a measure of how far the film has evolved towards steady state. Figure 9a confirms our hypothesis that shear is important near the corner. A lobe of high shear stress centered around ($\xi = 0$, $\eta = h$) demonstrates that, despite the symmetry boundary condition favouring normal stress, shear is introduced by the geometry in the region where the film experiences the largest change in direction. This effect is not captured by unidirectional-flow models, where the only source of shear is a solid boundary.
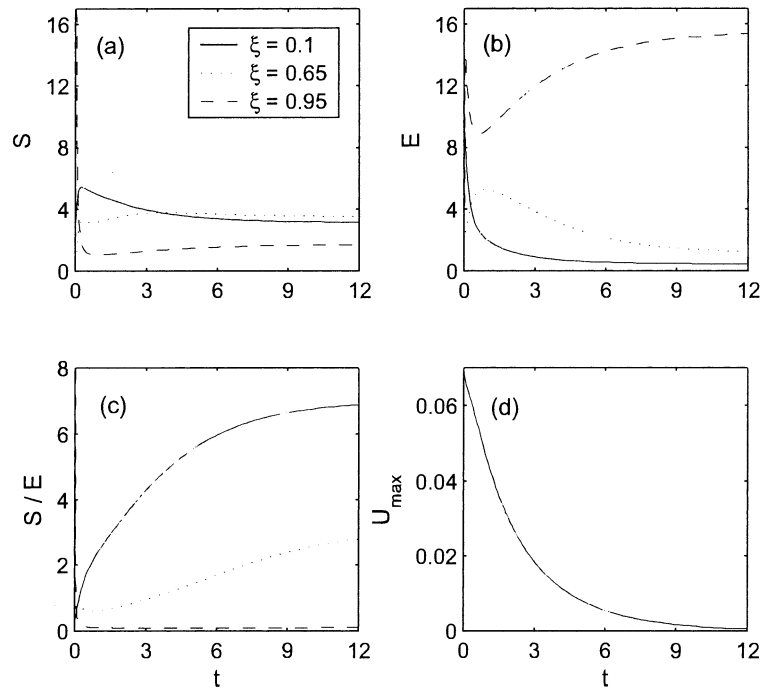
Figure 10. Evolution of (a) the shear stress S, (b) the extensional stress E, and (c) their ratio S/E for a free film in a corner with $\varepsilon = 0\cdot15$. The stresses are shown for three points ($\xi = 0\cdot1$, $0\cdot65$ and $0\cdot95$) at the free surface ($\eta = h$). Also shown (d) is the maximum velocity U_{max} as function of time, which was used to normalize S and E. Note from (c) that normal stress dominates over shear stress away from the corner ($\xi = 0\cdot95$), while the opposite is true close to the corner ($\xi = 0\cdot1$).

The viscous normal stresses, arising as the fluid is pulled towards the corner, are small near $\xi = 0$ (Figure 9b,e), making shear stress dominant as the fluid negotiates the corner. The region of the film dominated by shear is clearly visible in the contours of S/E (Figure 9c,f). Two smaller lobes of high shear are visible near the boundaries $\xi = \pm1$, while the regions furthest from the corner are extensionally dominated (Figure 9b,e). While the details depend on the initial condition, it is clear from Figure 9a,d that, as the film evolves, the region of high shear near the corner broadens and the maximum shear relaxes. In this process, the remaining two lobes of high shear get squeezed further towards the boundaries.

Figure 10 presents the time evolution of shear stress, normal stress and their ratio for $\varepsilon = 0\cdot15$ at three points in the flow field. The three points correspond to the free surface $\eta = h$ at $\xi = 0\cdot1$, $0\cdot65$ and $0\cdot95$. Also plotted is the evolution of the maximum instantaneous velocity U_{max}. This was used to normalize S and E at each time, thus removing the overall decay associated with the decrease in magnitude of the velocity field as the film approaches steady state. Figure 10c shows that the shear stress is larger than the normal stress close to the corner ($\xi = 0\cdot1$). Shear stress at the corner relaxes over time (Figure 10a), but normal stress relaxes faster (Figure 10a). Therefore, the relative importance of shear increases as the film evolves, reaching $S/E \approx 7$ at $t = 12$ (Figure 10c). This demonstrates that – despite the absence of a solid wall – the sudden change in direction is sufficient to make the flow shear-dominated near the corner. Far from the corner ($\xi = 0\cdot95$), normal stress prevails over shear stress. This region loosely corresponds to the extensional regime in the droplet pinch-off model by Eggers and Dupont [21], where $E \gg S$. It is enlightening to briefly compare the Eggers-

Dupont approach with ours. Instead of rescaling the equations and expanding the dependent variables in powers of ε as we have done in the present study, Eggers and Dupont expand in even powers (due to symmetry) of the 'thin' coordinate, η in our case. Thus, for example, $u = A_0 + A_2\eta^2 + A_4\eta^4 + \cdots$, where the A_i's are functions only of the 'long' coordinate, ξ. This simplifies the algebra and can be implemented in Cartesian coordinates (or in the $r - z$ planes in cylindrical coordinates), where there are no position-dependent terms in the equations of motion. However, in hyperbolic coordinates, if the position-dependent terms are retained in full as in the present study, the equations of motion cannot be integrated using this method. On the other hand, the current approach can be mapped onto a Taylor expansion in even powers of η by expanding the position-dependent terms as well as the derivatives in powers of ε. In this latter case, we find that the governing equations are in agreement with those obtained via Eggers and Dupont's expansion. Unfortunately, though this simplifies the equations, it again introduces a coordinate singularity in the corner.

Figure 10c summarizes the balance of shear and normal stress. In the intermediate region (*e.g.*, $\xi = 0.65$), shear and normal stresses are both important, their detailed distribution depending on the evolution of the three lobes of high shear observed in Figure 9a,d.

6. Discussion

We have investigated two configurations in which viscosity counteracts gravity and surface tension in governing the evolution of a thin film of liquid in a corner-region. In SH, we saw that when a no-slip boundary condition is imposed, as is typical for flow over topography, a single evolution equation is sufficient to solve the problem to lowest order. Both the geometry and the boundary condition then favor shear over normal stresses, as expected also for a unidirectional film over a solid substrate. On the other hand, when the two sides of the corner are axes of symmetry instead of rigid walls, two evolution equations are required to leading order and the velocity field is plug flow in the hyperbolic coordinates. In this case, shear and normal stresses are both important in some part of the flow domain, with shear prevailing near the corner. This balance is a result of the flow geometry and is therefore not captured by unidirectional-flow models.

With respect to more general lubrication approaches developed for thin films over topography [16, 17], ours has the advantage of being conceptually simpler and easier to implement. More important, our method is specifically tailored to a sharp corner. These advantages come at a price – namely flexibility, as our calculations are limited to the case of a square corner (but could be generalized to a corner of any angle with some patience). In previous studies, this configuration leads to a singularity in the substrate curvature and hence a singularity in the evolution equations. While this singularity could in principle be subdominant, thereby only minimally affecting the results, working in hyperbolic coordinates avoids the issue altogether. One could argue that, instead of this singularity, we have introduced another, associated with the U/ξ term in Equation (29). However, this is a completely separate issue, as this second singularity arises from the symmetry condition, not from the coordinate system, and would be present in any plug flow approximation. Indeed, no such singularity exists in the no-slip case (SH). Our approach could, in principle, be generalized to encompass a more general and flexible coordinate system, however the equations of motion become algebraically very complicated for symmetry boundary conditions, in which the gradient of the velocity appears in the boundary condition, rather than velocity itself. The simplicity of our formulation relies

partly on the fact that the symmetry axes are coordinate lines, ensuring a simple formulation of the boundary condition.

The price to pay for avoiding coordinate-induced singularities due to the sharp change in direction associated with a corner-region, is that we must retain ε in the final evolution equations (or, alternatively, in the initial condition). In most formulations, albeit not all [25], this does not occur. The reason for retaining ε in the position-dependent terms is that lubrication theory is based on the relative magnitude of variations in the dependent variables, that is derivatives. No assumptions are made about quantities that depend on position alone. Note that this is a non-issue in Cartesian coordinate, as purely position-dependent terms never arise. Take, for example, $(\xi^2 + \varepsilon^2 h^2)^{-1/2}$ in Equation (20). Whenever $|\xi| \gg \varepsilon h$, it is clearly allowed to approximate this expression by $|\xi|^{-1}$. However, this approximation is not valid at $\xi = 0$ and, even worse, introduces a singularity at the origin. The latter singularity reflects the singularity arising in the formulations mentioned above due to the gradient of the curvature of the substrate. These formulations are recovered if ε is set exactly to zero in our equations. While one may not call our approach 'standard lubrication theory' due to this perhaps spurious retention of the expansion parameter ε, it is nevertheless clear that our formulation provides a straightforward way of dealing with a geometry that is taboo for most other methods, without resorting to the full Stokes equations. For this reason, the filling fraction remains as a parameter, through ε.

In particular, we have not expanded the scale factors in the mass conservation equation (12) in powers of ε. Since we were lucky enough to be able to evaluate all integrals analytically, expansion in ε was not necessary and the resulting equations ensure exact mass conservation. In SH, we took a different approach and expanded the position-dependent terms as well, except for those arising in the mass conservation equation. We showed that the 'full' equations converge to this approximation as $\varepsilon \to 0$. This appears to indicate that, for arbitrarily small filling fraction, the integral contribution to the film evolution of the point-wise singularity due to the coordinate system is subdominant.

We also note that, in contrast to the no-slip boundary condition case, Moffatt eddies [20] can never form in the present configuration, as neither of the two axes is a solid wall. Thus, the lubrication approximation is likely to be close to the true physical solution as we need not include higher order terms to account for a change in direction in the flow. We are also safe from Moffatt eddies in future applications to filament stretching, where one of the two walls is solid; in this case, for Newtonian flows, eddies can form only for corners of angle smaller than 78°.

As mentioned in the introduction, a promising application of these corner flows is the expansion of a two-dimensional foam (Figure 1a), where the Plateau borders separating air bubbles can be conveniently modelled as a thin liquid film symmetric in both Cartesian directions. In this case, the fact that the domain stretches in time [11] must be taken into account by rescaling the equations with the instantaneous length of the side of a foam cell and imposing an integral constraint on the volume of liquid. Due to its inherent simplicity, our method would allow solutions for the shape of the interface at very long times. After the film has thinned considerably, down to a few tens of nanometers, an extra body force associated with the van der Waals forces must be included in the model to investigate rupture. These long-range molecular forces act to destabilize the film and are often modelled by a potential that depends on the negative third power of the film thickness [5, 7] (although several alternative formulations are in use, as summarized by Oron and coworkers [4]). On the other hand, electric double-layer forces can retard rupture, leading to black films [5]. Rupture is expected

to depend on the size of the system, which sets a limit on the most unstable wavelength [4, 26]. One could incorporate these effects into our model, and thus investigate rupture of liquid filaments between two bubbles. Such studies, despite the fact that they are strictly valid only for very idealized models of foam, would be of particular interest as to date numerical schemes cannot accurately resolve the liquid filaments for long times. This constitutes an important open question, regarding the material properties of foam.

An application that is further afield, but which originally motivated the present work is the 'fishbone' instability observed in filament stretching experiments performed on polystyrene-based Boger fluids by Spiegelberg and McKinley [27]. Instabilities of non-Newtonian fluids are important in the dynamics of paints, glues, lubricants and biological liquids. The base state is sketched in Figure 1d, while pictures of the instability can be found in [27]. This instability occurs at the corner between two orthogonally intersecting thin films, and is believed to arise from the competition of elastic and viscous stresses. A satisfying mechanistic explanation of the instability is yet to be determined. A complete investigation of this phenomenon would require three major modifications. First, the asymmetric stretching of the domain must be taken into account (*e.g.* only along y, not along x). Second, the non-Newtonian stress tensor could potentially make the analytical integration of mass conservation more difficult. Lubrication theory with non-Newtonian fluids has been developed for fiber-drawing using a viscoelastic fluid [28], for one-dimensional filaments using an Oldroyd-B constitutive model [29], and for a planar, unidirectional film using a power-law liquid [30]. In general, we expect one or more additional evolution equations associated with the constitutive equation of the fluid. Third, 'mixed' boundary conditions must be used – *i.e.*, no slip along the bottom and symmetry across the vertical axis. Thus, the evolution equations derived in this paper would be applied for $\xi < 0$, while the formulation from SH for the no-slip case would be applied for $\xi > 0$. Note that this is not the same as matching two solutions, since we simply use one or the other formulation in the numerical scheme, depending on the sign of ξ. A linear stability analysis would then have to be performed numerically to capture the 'fishbone' instability observed by Spiegelberg and McKinley [27]. We did not perform a stability analysis on our current Newtonian solution as the experiments exhibit no instability when Newtonian fluids are used [27]. With these modifications, our model could describe the stretching of a thin non-Newtonian film in a corner and potentially provide a mechanistic explanation of Spiegelberg and McKinley's fishbone instability.

7. Conclusions

We have shown that lubrication theory can be used to describe the evolution of a free film in a corner by adopting hyperbolic coordinates. The liquid film is then everywhere thin in the co-ordinate direction that points away from the axes of symmetry. The lubrication approximation gives two coupled nonlinear evolution equations for the film thickness and its velocity profile, plug flow, to leading order. While additional physico-chemical effects such as Van der Waals forces may be implemented, we restricted the model to free films evolving under viscosity, surface tension and gravity. In particular, we were able to compute shear and normal stresses. Far from the corner normal stress dominates, as expected. On the other hand, near the corner shear stresses prevail, due to the sharp change of direction the film is forced to undertake. We hope that this model will be useful as a starting point to further investigate the flow of free

films in corner regions, in particular the rupture of liquid threads in foams and the instabilities of viscoelastic fluids in stretching geometries.

A. Appendix: Details of the hyperbolic coordinate system

The following (dimensional) expressions were used to derive the governing equations in the hyperbolic coordinate system $\xi = x^2 - y^2$, $\eta = 2xy$:

$$y = \left(\frac{r - \xi}{2}\right)^{1/2}, \qquad x = \left(\frac{r + \xi}{2}\right)^{1/2}, \tag{A1}$$

$$\frac{\partial x}{\partial \eta} = -\frac{\partial y}{\partial \xi} = \frac{y}{2r}, \qquad \frac{\partial x}{\partial \xi} = \frac{\partial y}{\partial \eta} = \frac{x}{2r}, \tag{A2}$$

$$f_1 = \frac{1}{s}\frac{\partial s}{\partial \xi} = -\frac{\xi}{2r^2}, \qquad f_2 = \frac{1}{s}\frac{\partial s}{\partial \eta} = -\frac{\eta}{2r^2}. \tag{A3}$$

The unit outward normal and tangent vectors are, respectively,

$$\hat{\boldsymbol{n}} = \frac{-h'\hat{\boldsymbol{\xi}} + \hat{\boldsymbol{\eta}}}{(1 + h'^2)^{1/2}}, \qquad \hat{\boldsymbol{t}} = \frac{\hat{\boldsymbol{\xi}} + h'\hat{\boldsymbol{\eta}}}{(1 + h'^2)^{1/2}}. \tag{A4}$$

Using Equation (7a) to compute the gradient of the velocity field, we obtain the following expression for the Newtonian stress tensor $\boldsymbol{\Pi}$ in Equation (3)

$$\boldsymbol{\Pi} = \begin{pmatrix} -p + \dfrac{2\mu}{s}\left(\dfrac{\partial u}{\partial \xi} - \dfrac{\eta v}{2r^2}\right) & \dfrac{\mu}{s}\left(\dfrac{\partial v}{\partial \xi} + \dfrac{\partial u}{\partial \eta} + \dfrac{\eta u + \xi v}{2r^2}\right) \\ \dfrac{\mu}{s}\left(\dfrac{\partial v}{\partial \xi} + \dfrac{\partial u}{\partial \eta} + \dfrac{\eta u + \xi v}{2r^2}\right) & -p + \dfrac{2\mu}{s}\dfrac{\partial v}{\partial \eta} - \dfrac{\xi v}{2r^2} \end{pmatrix} \tag{A5}$$

The unit vectors in hyperbolic coordinates along ξ and η are

$$\hat{\boldsymbol{\xi}} = \left(\frac{x}{\sqrt{r}}, -\frac{y}{\sqrt{r}}\right), \qquad \hat{\boldsymbol{\eta}} = \left(\frac{y}{\sqrt{r}}, \frac{x}{\sqrt{r}}\right). \tag{A6}$$

The unit vectors in Cartesian coordinates along x and y are

$$\hat{\boldsymbol{j}} = \frac{1}{s}\frac{\partial x}{\partial \xi}\hat{\boldsymbol{\xi}} + \frac{1}{s}\frac{\partial x}{\partial \eta}\hat{\boldsymbol{\eta}}, \qquad \hat{\boldsymbol{k}} = \frac{1}{s}\frac{\partial y}{\partial \xi}\hat{\boldsymbol{\xi}} + \frac{1}{s}\frac{\partial y}{\partial \eta}\hat{\boldsymbol{\eta}}. \tag{A7}$$

References

1. K. Kumar, A. D. Nikolov and D. T. Wasan, Effect of film curvature on drainage of thin liquid films. *J. Colloid Interf. Sci.* 256 (2002) 194–200.
2. S. Hilgenfeldt, S. A. Koehler and H. A. Stone, Dynamics of coarsening foams: accelerated and self-limited drainage. *Phys. Rev. Letters* 86 (2001) 4704–4707.
3. A. L. Bertozzi and M. C. Pugh, Long-wave instabilities and saturation in thin film equations. *Comm. Pure Appl. Math.* 51 (1998) 625–661.
4. A. Oron, S. H. David and S. G. Bankoff, Long-scale evolution of thin liquid films. *Rev. Mod. Phys.* 69 (1997) 931–980.
5. T. Erneux and S. H. Davis, Nonlinear rupture of free films. *Phys. Fluids A* 5 (1993) 1117–1122.
6. M. Prevost and D. Gallez, Nonlinear rupture of thin free liquid films. *J. Chem. Phys.* 184 (1986) 4043–4048.
7. M. B. Williams and S. H. Davis, Nonlinear theory of film rupture. *J. Colloid. Interf. Sci.* 90 (1982) 220–228.
8. A. Vrij, Possible mechanisms for the spontaneous rupture of thin, free liquid films. *Discuss. Faraday Soc.* 42 (1966) 23–33.
9. F. Brochard Wyart and J. Daillant, Drying of solids wetted by thin liquid films. *Can. J. Phys.* 68 (1990) 1084–1088.
10. F. Brochard Wyart, P. Martin and C. Redon, Liquid/liquid dewetting. *Langmuir* 9 (1993) 3682–3690.
11. C. Pozrikidis, Expansion of a two-dimensional foam, *Eng. Analysis with Boundary Elements* 26 (2002) 495–504.
12. S. Kalliadasis, C Bielarz and G. M. Homsy, Steady free-surface thin film flows over topography. *Phys. Fluids* 12 (2000) 1889–1898.
13. A. Mazouchi and G. M. Homsy, Free surface stokes flow over topography. *Phys. Fluids* 13 (2001) 2751–2761.
14. L. D. Landau and B. Levich, Dragging of a liquid by a moving plate. *Acta Physicochimica U.R.S.S.* 17 (1942) 42–54.
15. R. J. Braun, S. A. Snow and S. Naire, Models for gravitationally-driven free-film drainage. *J. Eng. Math.* 43 (2002) 281–314.
16. L. W. Schwartz and D. E. Weidner, Modeling of coating flows on curved surfaces. *J. Engng. Math.* 29 (1995) 91–103.
17. R. V. Roy, A. J. Roberts and M. E. Simpson, A lubrication model of coating flows over a curved substrate in space. *Fluid Mech.* 454 (2002) 235–261.
18. R. Stocker and A. E. Hosoi, Lubrication in a corner. *J. Fluid Mech.* submitted (2003).
19. G. B. Arfken, *Mathematical Methods for Physicists.* San Diego: Academic Press (1970) 815pp.
20. H. K. Moffatt, Viscous and resistive eddies near a sharp corner. *J. Fluid Mech.* 18 (1963) 1–18.
21. J. Eggers and T. F. Dupont, Drop formation in a one-dimensional approximation of the Navier-Stokes equation. *J. Fluid Mech.* 262 (1994) 205–221.
22. M. Abramowitz and I. A. Stegun, *Handbook of Mathematical Functions: With Formulas, Graphs, and Mathematical Tables.* New York: Dover (1965) 1046pp.
23. W. H. Press, S. A. Teukolsky, W. T. Vetterling and B. P. Flannery, *Numerical Recipes in Fortran: The Art of Scientific Computing.* Cambridge: Cambridge University Press (1992) 963pp.
24. L. D. Landau and E. M. Lifschitz, *Fluid Mechanics* Oxford: Pergamon Press (1987) 539pp.
25. A. E. Hosoi and L. Mahadevan, Axial instability of a free surface front in a partially-filled rotating cylinder. *Phys. Fluids* 11 (1999) 97–106.
26. R. J. Gumerman and G. M. Homsy, The stability of radially bounded thin films. *Chem. Eng. Com.* 2 (1975) 27–36.
27. S. H. Spiegelberg and G. H. McKinley, Stress relaxation and elastic decohesion of viscoelastic polymer solutions in extensional flow. *J. Non-Newt. Fluid Mech.* 67 (1996) 49–76.
28. W. W. Schultz, Slender viscoelastic fiber flow. *J. Rheol.* 31 (1987) 733–750.
29. D. O. Olagunju, A 1-D theory for extensional deformation of a viscoelastic filament under exponential stretching. *J. Non-Newt. Fluid Mech.* 87 (1999) 27–46.
30. C. C. Hwang and S. H. Chang, Rupture theory of thin power-law liquid film. *J. Appl. Phys.* 74 (1993) 2965–2967.